Advances in Aircraft and Spacecraft Science, *Vol. 11, No. 4 (2024) 363-382*
https://doi.org/10.12989/aas.2024.11.4.363

Assessing the effect of stiffeners on the stability of sandwich metacomposite toroidal shells under axial compression

Farzad Ebrahimi*[1], Mohammadhossein Goudarzfallahi[2] and Ali Alinia Ziazi[2]

[1]*Department of Mechanical Engineering*, *Faculty of Engineering*, *Imam Khomeini International University*, *Qazvin*, *Iran*
[2]*Mechanical Engineering Department*, *Science and Research Branch*, *Islamic Azad University*, *Tehran*, *Iran*

(Received September 10, 2024, Revised December 21, 2024, Accepted December 23, 2024)

Abstract. This research explores the effect of stiffeners on the stability of sandwich toroidal shell segments (TSSs) featuring the recently developed graphene origami (GOri)-enabled auxetic metamaterial core and carbon nanotube (CNT)-reinforced face sheets supported by elastic foundations and subjected to axial compression. The shells are stiffened circumferentially or longitudinally with CNT-reinforced rings or stringers, which are internally embedded and modeled using an innovative smeared stiffener approach. CNTs are distributed throughout the thickness of the shell-stiffener structure, following either a uniformly distributed (UD) or functionally graded (FG) distribution model. The nonlinear equilibrium equations for the longitudinally shallow shells are derived using the von Kármán shell theory and Stein and McElman approximations while considering a Winkler-Pasternak elastic foundation to model the interaction between the shell and the elastic foundation. A deflection solution under simply supported boundary conditions is employed, and the Galerkin method is applied to obtain the nonlinear load-deflection relationship. This relationship is subsequently used to calculate the buckling loads and analyze the postbuckling behavior. The numerical analysis addresses the effects of stiffeners, considering the CNT volume fraction, distribution models, geometrical parameters, and the impact of the elastic foundation on the stability of auxetic-core TSSs.

Keywords: buckling and postbuckling; carbon nanotube-reinforced composite; origami-enabled auxetic metamaterial core; stiffener; toroidal shell segment

1. Introduction

Auxetic materials are gaining significant attention for research and application in various industries due to their lightweight and exceptional ability to absorb the impact impulses they are subjected to. Compression and shear resistance, energy absorption, low frequency and energy harvesting, and high damping resistance are only some of the mechanical attributes these metamaterials have been shown to improve (Ebrahimi 2024). Advanced composite materials can be developed by integrating an auxetic core layer into a sandwich-structured composite, enhancing its static and dynamic load-carrying capacity. This innovation proves highly beneficial in diverse applications, including civil engineering, aerospace engineering, and energy absorption systems. Numerous previous studies have investigated the mechanical performance of plate and shell structures incorporating auxetic cores. Using thick shell theory, Thang *et al.* (2024) conducted a

*Corresponding author, Professor, E-mail: febrahimy@eng.ikiu.ac.ir

http://www.techno-press.org/?journal=aas&subpage=7 ISSN: 2287-528X (Print), 2287-5271 (Online)

vibration analysis of sandwich shells with a barrel shape comprising an auxetic honeycomb core. Ebrahimi *et al.* (2023) investigated the vibration response of a composite cylindrical shell comprising an auxetic core supported by an elastic foundation under axial compression and external excitation. The impact behavior of a porous, doubly-curved shell with an auxetic honeycomb core was examined by Fu *et al.* (2023), based on shear deformation theory.

Carbon nanotubes (CNTs) are highly suitable for enhancing composite materials because of their outstanding thermal, mechanical, and electrical characteristics. When incorporated as fibers, they can be distributed within a polymeric matrix in a manner that is either uniform (UD) or functionally graded (FG) (Ebrahimi and Dabbagh 2020). Using a perturbation method and higher-order shear deformation theory, Shen (2011) conducted a postbuckling analysis of CNT-reinforced cylindrical shells subjected to axial loading in a thermal environment. Sofiyev and Kuruoglu (2022) studied buckling in conical shells reinforced by CNTs under hydrostatic pressure and axial compression on an elastic foundation. Torabi and Ansari (2018) studied the effects of thermal loading on the vibration and buckling behavior of FG-CNTRC conical shells. Cho (2023) investigated the vibration behavior of FG-CNTRC cylindrical shell panels supported by an elastic foundation. Further studies on nanocomposite structures have been conducted by Al-Houri *et al.* (2024).

Graphene, discovered in 2004, is a two-dimensional material that is just one atom thick and has a high ratio of surface area to thickness. Carbon atoms are joined by bundles to form a graphene sheet's structure, which repeats as a hexagon. Excellent mechanical strength, heat conduction, and electrical conduction have all been demonstrated by this nanostructure. The mechanical properties of the graphene layer have been observed, revealing that it is even more rigid than stainless steel in two dimensions. In the majority of simulations, the graphene sheet's elasticity modulus is reported to be around 1 TPa (Ebrahimi 2015). As a result of such intriguing characteristics, graphene may be considered a highly promising option for the reinforcement of composites, leading to the development of a new type of nanocomposite material identified as FG graphene-reinforced composite (FG-GRC) (Shen 2017). Subsequently, research was conducted on the thermal and mechanical properties of GRC structures (Sahmani and Aghdam 2017, Shen and Xiang 2018a, Shen and Xiang 2018b, Dong *et al.* 2018, Zhou *et al.* 2019, Ebrahimi *et al.* 2024a, Ebrahimi and Ezzati 2024, Xu and She 2023, Wang *et al.* 2020).

Recently, there has been a surge in the popularity of utilizing the traditional paper craft of origami, which involves folding paper (the Japanese terms 'ori' meaning 'fold' and 'gami' meaning 'paper'). This resurgence is particularly notable in the creation of mechanical metamaterials. The folding of basic two-dimensional thin-film materials makes it possible to convert them into intricate three-dimensional structures with distinctive and adjustable mechanical characteristics. These properties include flexibility, tunable Poisson's ratio, and adjustable stiffness (Kamrava *et al.* 2017, Kolken and Zadpoor 2017, Zhai *et al.* 2021). Motivated by the Miura-origami metamaterial and graphene origami (GOri), a novel category of GOri-enabled metallic metamaterials (GOEAMs) that possess enhanced characteristics has been developed by Zhao *et al.* (2022a). These Metamaterials exhibit tunable NPR and improved mechanical properties. The research indicates that the adjustability of NPR is attainable by altering the content of graphene, graphene folding degree, and temperature. Additionally, micromechanical models assisted by genetic programming (GP) have been developed to predict the mechanical characteristics of the GOEAMs precisely. Zhao *et al.* (2022b) studied beams' dynamic responses and free vibration behavior composed of a unique combination of GOEAMs. These beams exhibit an auxetic property, and their dynamic characteristics are effectively controlled by the content of

graphene as well as the folding degree of GOri, both of which vary across the thickness of the beams. The research findings demonstrated that the inclusion of GOri allows for a high degree of tunability in beams. In another study, Zhao *et al.* (2022c) examined the buckling and postbuckling characteristics of GOEAM beams. Ebrahimi and Parsi (2023) investigated the propagation of waves in GOEAM beams. Ebrahimi and Ahari (2024) investigated the buckling behavior of a composite material with magnetostrictive face sheets and GOri-enabled features. Jin *et al.* (2024) studied the vibrational behavior of a GORI doubly curved shell. Studies on the vibration and stability characteristics of GOEAM beams submerged in fluids were conducted by Murari *et al.* (2024).

Toroidal shell segments (TSSs) are widely used in various engineering fields, including aeronautical, underwater, and civil structures. Buckling analysis for these types of shells of revolution, composed of modern composite materials, has received significant attention in the last few years. Nguyen *et al.* (2023) investigated the buckling and postbuckling analysis of TSSs with re-entrant honeycomb auxetic cores and GRC coatings subjected to torsional loads. They employed von Karman-Donnell shell theory and the Stein and McElman approximations (Stein and McElman 1965) to derive the equilibrium equations for shells with longitudinally shallow curvature surrounded by an elastic foundation. They utilized the Galerkin procedure to present the governing equations. Ebrahimi *et al.* (2024b) conducted a comparative stability analysis of sandwich TSSs using a composite material with a GOREAM core and CNTRC face sheets. The results showed that the GOREAM core significantly enhanced stability compared to re-entrant auxetic metamaterials.

Porosity, a typical manufacturing occurrence that can significantly degrade the efficiency of mechanical structures by affecting stiffness, Young's modulus, and density, was further explored by Ebrahimi *et al.* (2024c). They examined the impact of porosity on the stability of sandwich TSSs with a GOREAM core and porous FG-CNT face sheets. Tien *et al.* (2022) studied honeycomb auxetic-core sandwich TSSs with CNT-reinforced face sheets under radial pressure. In similar research, Phuong *et al.* (2023) investigated the buckling and postbuckling behavior of TSSs composed of a re-entrant honeycomb core and GRC face sheets subjected to radial loads. Hieu and Tung (2020) studied the buckling and postbuckling analysis of CNRC TSSs subjected to combined thermal and mechanical. Nam *et al.* (2022) analyzed nonlinear buckling in sandwich TSSs with re-entrant honeycomb and graphene-reinforced face sheets under axial loads.

Utilizing stiffeners that possess optimal geometrical and mechanical properties is a practical approach to improving the buckling behavior of shell structures. Reddy and Starnes (1993) studied the effect of axial and circumferential stiffeners on the buckling loads of composite cylindrical shells. Wang *et al.* (2016) conducted a study on the buckling behavior of stiffened composite cylindrical shells by introducing an effective smeared stiffener method. Phuong*et et al.* (2020) developed an enhanced smeared stiffener technique to study the nonlinear buckling and postbuckling performance of FG-GRC cylindrical shells. These shells were reinforced with FG-GRC laminated stiffeners and subjected to external pressure. Dong *et al.* (2022) examined CNTR cylindrical shells' stability, reinforced with longitudinal or circumferential CNTR stiffeners under axial compression and thermal conditions within an elastic medium. In a separate study, Dong *et al.* (2023) investigated the buckling performance of CNTRC cylindrical shells with CNTRC stiffeners subjected to external pressure. In light of stiffeners' influence on TSSs, Dao *et al.* (2016) examined buckling analysis of eccentrically stiffened FG TSSs under radial, axial, and hydrostatic pressure. Vuong and Duc (2018) examined the nonlinear buckling of TSSs with FGM stiffeners under radial pressure. Using the same stiffener concept as Phuong *et al.* (2020), Minh *et al.* (2022)

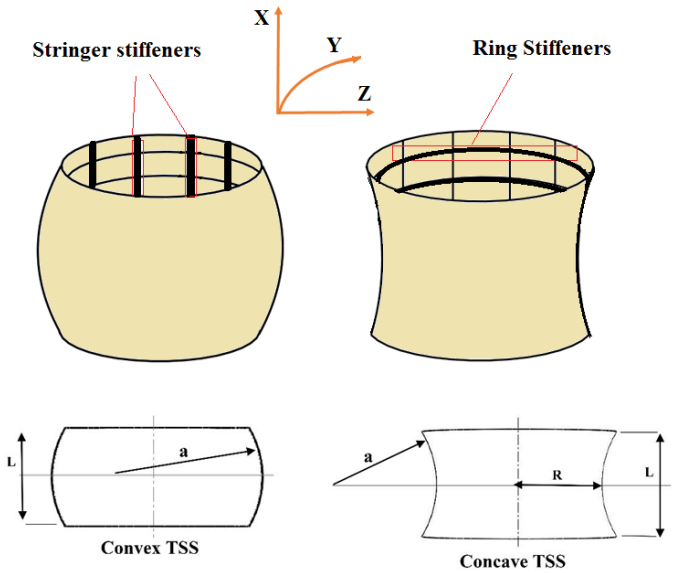

Fig. 1 Configuration of stiffened convex and concave TSSs

focused on CNTRC TSSs stiffened with FG-CNTRC rings or stringers, while Cao *et al.* (2023) examined stiffened piezoelectric FG-GRCL TSSs in thermal environments.

A comprehensive review of the existing literature on TSSs reveals that, despite numerous prior studies on various aspects of TSSs under different loading conditions, the influence of advanced auxetic cores and stiffeners on the stability of these structures remains inadequately addressed. This study aims to explore the effects of stiffeners on the buckling and postbuckling characteristics of sandwich-structured composite TSSs incorporating the recently developed GOEAM core and CNT-reinforced coatings. The analysis approach for stiffened FG-CNTRC TSSs is presented using the smeared stiffener technique proposed by Phuong *et al.* (2020). The shells are subjected to axial compression and are surrounded by Pasternak's elastic foundations. The fundamental governing equations are established by combining the von Kármán kinematic nonlinearity with the Stein and McElman approximation and subsequently solved using the Galerkin method. The effects of FG-CNTRC stiffeners, including stiffener types, CNT content and its various distribution patterns, geometrical parameters, and the presence of an elastic foundation, are investigated through parametric analysis. This study's findings have significant practical implications for designing and optimizing more stable structures with higher stiffness-to-weight ratios used in aerospace, civil engineering, and marine industries.

2. Section title: Level 1

2.1 CNT-reinforced face sheets

Fig. 1 illustrates the geometry of stiffened auxetic-core sandwich-structured TSSs with concave (exhibiting negative Gaussian curvature) and convex (showing positive Gaussian curvature) configurations. The shells have doubly curved geometry and are based on a complex coordinate

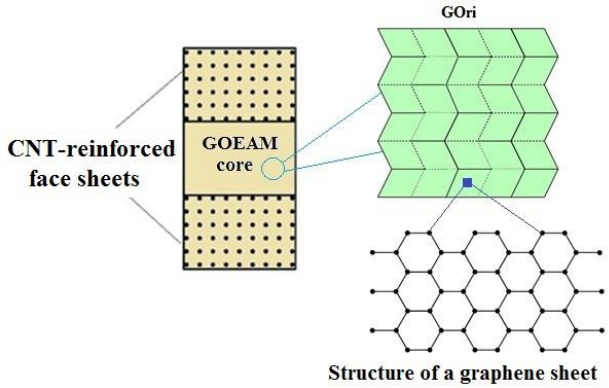

Fig. 2 Configuration of sandwich composite structure with GOEAM core layer and CNTRC face sheets

system. The schematic representation of the sandwich-structured composite is also presented in Fig. 2. As illustrated, the face sheets of the sandwich-structured TSSs are reinforced with CNTs through the thickness. This study considers three types of CNT distributions for the face sheets: uniform distribution (UD), FG-X, and FG-O. Furthermore, this research examines the direction of CNT reinforcement from both circumferential and longitudinal perspectives. The volume fractions of CNTs in the face sheets can be represented as (Shen 2011)

$$V_{CNT} = \bar{V}_{CNT} \qquad \text{(UD)}$$

$$V_{CNT} = \left(\frac{4|z|}{h_1}\right)\bar{V}_{CNT} \qquad \text{(FG-X)} \tag{1}$$

$$V_{CNT} = \left(2 - \frac{4|z|}{h_1}\right)\bar{V}_{CNT} \qquad \text{(FG-O)}$$

where h_1 is the thickness of face sheets. The extended rule of mixture is used for determining the elastic constants of orthotropic materials in the CNT-reinforced face sheets as follows (Shen 2011)

$$\begin{aligned} E_{11}^{CNTRC} &= V_{ma}E_{ma} + \eta_1 V_{CNT}E_{11}^{CNT} \\ E_{22}^{CNTRC} &= \frac{\eta_2}{\frac{V_{CNT}}{E_{22}^{CNT}} + \frac{V_{ma}}{E_{ma}}} \\ G_{12}^{CNTRC} &= \frac{\eta_3}{\frac{V_{CNT}}{G_{12}^{CNT}} + \frac{V_{ma}}{G_{ma}}} \\ \nu_{12}^{CNTRC} &= V_{ma}\,\nu_{ma} + V_{CNT}\,\nu_{12}^{CNT} \end{aligned} \tag{2}$$

in which E_{11}^{CNT}, E_{22}^{CNT}, and G_{12}^{CNT} represent the elastic moduli for the CNTs, while E_{ma} and G_{ma} denote the elastic moduli of the matrix material. Additionally, η_j (j=1, 2, 3) is the CNT performance parameter, and V_{CNT} and V_{ma} are the CNT and matrix volume fractions, satisfying the relationship $V_{\mathrm{CNT}} + V_{ma} = 1$. Furthermore, Poisson's ratios for the CNTs and matrix materials are referred to as ν_{12}^{CNT} and ν_{ma}, respectively.

2.2 Mechanical characteristics of the GOEAM Core

In this study, the innovative auxetic metamaterial known as GOEAM is utilized as the core layer of a sandwich-structured composite material. Fig. 2 illustrates a schematic of the GOEAM-core layer with CNT-reinforced face sheets. The mechanical characteristics of GOEAM can be presented as follows (Zhao *et al.* 2022a)

$$\begin{gathered} E_c = \frac{1+\xi\eta\, V_{Gr}}{1-\eta V_{Gr}} E_{Cu} \times f_E(H_{Gr}, V_{Gr}, T) \\ \nu_c = (\nu_{Gr} V_{Gr} + \nu_{Cu} V_{Cu}) \times f_\nu(H_{Gr}, V_{Gr}, T) \\ \alpha_c = (\alpha_{Gr} V_{Gr} + \alpha_{Cu} V_{Cu}) \times f_\alpha(V_{Gr}, T) \\ \rho_c = (\rho_{Gr} V_{Gr} + \rho_{Cu} V_{Cu}) \times f_\rho(V_{Gr}, T) \end{gathered} \tag{3}$$

In which η and ξ are material coefficients and size coefficients, respectively, as presented by Zhao *et al.* (2022a)

$$\begin{gathered} \eta = \frac{(E_{Gr}/E_{Cu}) - 1}{(E_{Gr}/E_{Cu}) + \xi} \\ \xi = 2(l_{Gr}/t_{Gr}) \end{gathered} \tag{4}$$

where l_{Gr} and t_{Gr} represent the dimensions of graphene, with l_{Gr} referring to its length and t_{Gr} referring to its thickness, f_E, f_ν, f_α, and f_ρ are the modification functions, expressed as (2022a)

$$\begin{gathered} f_E(H_{Gr}, V_{Gr}, T) = 1.11 - 1.22V_{Gr} - 0.134\left(T/T_0\right) + 0.559V_{Gr}\left(T/T_0\right) - 5.5H_{Gr}V_{Gr} + \\ 38H_{Gr}V_{Gr}^2 - 20.6H_{Gr}^2V_{Gr}^2 \\ f_\nu(H_{Gr}, V_{Gr}, T) = 1.01 - 1.43V_{Gr} + 0.165\left(T/T_0\right) - 16.8H_{Gr}V_{Gr} - 1.1H_{Gr}V_{Gr}\left(T/T_0\right) + \\ 16H_{Gr}^2V_{Gr}^2 \\ f_\alpha(V_{Gr}, T) = 0.794 - 16.8V_{Gr}^2 - 0.0279\left(T/T_0\right)^2 + 0.182\left(T/T_0\right)(1+V_{Gr}) \\ f_\rho(V_{Gr}, T) = 1.01 - 2.01V_{Gr}^2 - 0.0131\left(T/T_0\right) \end{gathered} \tag{5}$$

Furthermore, T_0 is equivalent to 300 K and T represents ambient temperature.

2.3 The stiffener structure

As depicted in Fig. 1, the TSSs are stiffened longitudinally with stringers and circumferentially with rings. Additionally, Fig. 3 illustrates the cross-section of the shell-stiffener structure in longitudinal and circumferential directions, in which the CNT-reinforced stringer and ring CNT-reinforced TSSs are internally reinforced by CNT-reinforced stringer and ring stiffeners. According to the improved smeared stiffener technique Phuong *et al.* (2020) developed, the FG-CNTRC laminated TSSs are assumed to be reinforced with closely spaced rings and stringers. The detachment of the TSSs and stiffeners can be minimized by ensuring material continuity between the shell and stiffener structures. This paper proposes FG-CNTRC stiffeners with distribution patterns similar to those in the shell, i.e., UD, FG-X, and FG-O CNTRC stiffeners. Furthermore, the CNT orientation is consistent in both the face sheets and stiffeners, with the same distribution at the contact surfaces of the shell-stiffener structure. The distribution models of CNTs in the stiffeners are obtained by adjusting h to h_s and z to $z - h/2 - h_s/2$ in Eq. (1).

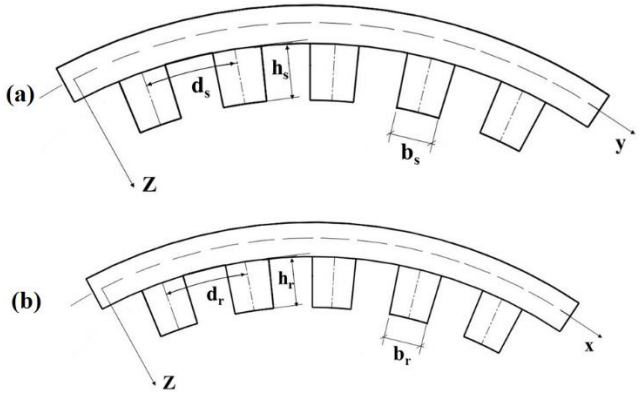

Fig. 3 Cross sections of stiffened TSSs: (a) stringer-stiffened shell and (b) ring-stiffened shell

3. Fundamental equations

The governing equations describing the stability of stiffened sandwich TSSs considering the GOEAM core and CNT-reinforced face sheets subjected to a uniform axial compressive load surrounded by an elastic foundation can be derived from the von Karman-Donnell theory. Fig. 1 illustrates how TSSs are located within a complex coordinate system with doubly curved geometry. The shallowness of the TSSs along the meridian allows the application of the Stein and McElman approximation (1965), simplifying the governing equations for the shells. The mid-surface strain components are presented as (Stein and McElman 1965)

$$\begin{aligned}\varepsilon_x^0 &= \frac{\partial u}{\partial x} + \left(\frac{\partial w}{\partial x}\right)^2 - \frac{w}{a}\\ \varepsilon_y^0 &= \frac{\partial v}{\partial x} + \left(\frac{\partial w}{\partial y}\right)^2 - \frac{w}{R}\\ \gamma_{xy}^0 &= \frac{\partial u}{\partial y} + \frac{\partial v}{\partial x} + \frac{\partial w}{\partial x}\frac{\partial w}{\partial y}\end{aligned} \tag{6}$$

Where u, v, and w are displacement components in the x, y, and z directions, respectively. Hooke's law for sandwich structure TSSs is defined as (Reddy 2003)

$$\begin{bmatrix}\sigma_x\\ \sigma_y\\ \sigma_{xy}\end{bmatrix} = \begin{bmatrix}Q_{11} & Q_{12} & 0\\ Q_{12} & Q_{22} & 0\\ 0 & 0 & Q_{66}\end{bmatrix}\begin{bmatrix}\varepsilon_x\\ \varepsilon_y\\ \gamma_{xy}\end{bmatrix} \tag{7}$$

where

$$\begin{aligned}Q_{11} &= \frac{E_{11}}{1-\nu_{12}\nu_{21}}\\ Q_{12} &= \frac{E_{11}\nu_{21}}{1-\nu_{12}\nu_{21}}\\ Q_{22} &= \frac{E_{22}}{1-\nu_{12}\nu_{21}}\\ Q_{66} &= G_{12}\end{aligned} \tag{8}$$

By integrating Eq. (7) over the thickness of the shell and stiffeners, the internal forces can be derived as follows

$$\begin{bmatrix} N_x \\ N_y \\ N_{xy} \\ M_x \\ M_y \\ M_{xy} \end{bmatrix} = \begin{bmatrix} A_{11} & A_{12} & 0 & B_{11} & B_{12} & 0 \\ A_{12} & A_{22} & 0 & B_{12} & B_{22} & 0 \\ 0 & 0 & A_{66} & 0 & 0 & B_{66} \\ B_{11} & B_{12} & 0 & D_{11} & D_{12} & 0 \\ B_{12} & B_{22} & 0 & D_{12} & D_{22} & 0 \\ 0 & 0 & B_{66} & 0 & 0 & D_{66} \end{bmatrix} \begin{bmatrix} \varepsilon_x^0 \\ \varepsilon_y^0 \\ \gamma_{xy}^0 \\ -w_{,xx} \\ -w_{,yy} \\ -2w_{,xy} \end{bmatrix} \tag{9}$$

where A_{ij}, B_{ij}, and D_{ij} are the total stiffness of the stiffened shell, which can be expressed as (Phuong *et al.* 2020)

$$\left(A_{ij}, B_{ij}, D_{ij}\right) = \left(A_{ij}^{sh}, B_{ij}^{sh}, D_{ij}^{sh}\right) + \left(A_{ij}^{s}, B_{ij}^{s}, D_{ij}^{s}\right) + \left(A_{ij}^{r}, B_{ij}^{r}, D_{ij}^{r}\right) \quad (i,j = 1,2,6) \tag{10}$$

where $A_{ij}^{sh}, B_{ij}^{sh}, D_{ij}^{sh}$ represent the sandwich-structured shell's stiffness and are calculated as

$$\left(A_{ij}^{sh}, B_{ij}^{sh}, D_{ij}^{sh}\right) = \int_{\Omega} \bar{Q}_{ij}\,(1, z, z^2)dz \tag{11}$$

where Ω represents the shell's thickness domain, and the stiffnesses of CNTR ring stiffeners can be obtained by using the expression Phuong *et al.* (2020)

$$\begin{bmatrix} A_{22}^r & B_{22}^r \\ B_{22}^r & D_{22}^r \end{bmatrix} = \begin{bmatrix} \tilde{A}_{22} & \tilde{B}_{22} \\ \tilde{B}_{22} & \tilde{D}_{22} \end{bmatrix} - \begin{bmatrix} \tilde{A}_{12} & 0 & \tilde{B}_{12} & 0 \\ \tilde{B}_{12} & 0 & \tilde{D}_{12} & 0 \end{bmatrix} \begin{bmatrix} \tilde{A}_{11} & 0 & \tilde{B}_{11} & 0 \\ 0 & \tilde{A}_{66} & 0 & \tilde{B}_{66} \\ \tilde{B}_{11} & 0 & \tilde{D}_{11} & 0 \\ 0 & \tilde{B}_{66} & 0 & \tilde{D}_{66} \end{bmatrix} \begin{bmatrix} \tilde{A}_{12} & \tilde{B}_{12} \\ 0 & 0 \\ \tilde{B}_{12} & \tilde{D}_{12} \\ 0 & 0 \end{bmatrix} \tag{12}$$

where

$$\left(\tilde{A}_{ij}, \tilde{B}_{ij}, \tilde{C}_{ij}\right) = \frac{b_r}{d_r} \int_{\Omega_r} \tilde{Q}_{ij}\,(1, z, z^2)dz \qquad (i,j = 1,2,6) \tag{13}$$

The calculation procedure can be similarly performed for stringer stiffeners by replacing subscript '22' with '11' and subscript '11' with '22' in Eqs. (10)-(12) and by replacing b_r and d_r with b_s and d_s respectively. The equilibrium equations for stiffened sandwich TSSs, while considering Winkler-Pasternak elastic foundation (with foundation stiffness coefficients denoted as K_1, K_2), can be expressed as follows (Nam *et al.* 2022)

$$\begin{gathered} N_{x,x} + N_{xy,y} = 0 \\ N_{xy,x} + N_{y,y} = 0 \\ M_{x,xx} + M_{y,yy} + 2M_{xy,xy} + N_x w_{,xx} + N_y w_{,yy} + 2N_{xy} w_{,xy} + \frac{N_x}{a} + \frac{N_y}{R} \\ -K_1 w + K_2\left(w_{,xx} + w_{,yy}\right) = 0 \end{gathered} \tag{14}$$

The Airy stress function $\varsigma(x, y)$ is defined as

$$\phi_{,xx} = N_y,\ \phi_{,yy} = N_x,\ \phi_{,xy} = -N_{xy} \tag{15}$$

It is evident that when three conditions (15) are satisfied, the first two equations in Eq. (14) are also satisfied. By inserting Eqs. (9) and (15) into the final equation of Eq. (14), the equilibrium equations are derived as

$$\begin{aligned} D_{11}w_{,xxxx} + D_{22}w_{,yyyy} + (D_{12} + D_{21} + 4D_{66})w_{,xxyy} - \frac{1}{R}\phi_{,xx} - \frac{1}{a}\phi_{,yy} - \phi_{,yy}w_{,xx} \\ - \phi_{,xx}w_{,yy} + 2\phi_{,xy}w_{,xy} + K_1 w - K_2\left(w_{,xx} + w_{,yy}\right) = 0 \end{aligned} \tag{16}$$

From Eq. (6), the compatibility equation is obtained as

$$\varepsilon^0_{x,yy} + \varepsilon^0_{y,xx} - \gamma^0_{xy,xy} + \frac{1}{R}w_{,xx} + \frac{1}{a}w_{,yy} - w^2_{,xy} + w_{,xx}w_{,yy} = 0 \tag{17}$$

Substituting Eq. (9) into the compatibility Eq. (11) yields

$$\bar{C}_{11}\,\phi_{,xxxx} + \bar{C}_{22}\,\phi_{,yyyy} + (\bar{C}_{66} - 2\bar{AC}_{12})\,\phi_{,xxyy} - w^2_{,xy} + w_{,xx}w_{,yy} + \frac{1}{R}w_{,xx} + \frac{1}{a}w_{,yy} = 0 \tag{18}$$

where

$$\bar{C}_{11} = \frac{A_{11}}{\Delta},\ \bar{C}_{22} = \frac{A_{22}}{\Delta},\ \bar{C}_{12} = \frac{A_{12}}{\Delta},\ \bar{C}_{66} = \frac{1}{A_{66}},\ \Delta = A_{11}A_{22} - A^2_{12} \tag{19}$$

Also, the closed condition of the shell necessitates that

$$\int_0^{2\pi R}\int_0^{L} v_{,y}\,dxdy = \int_0^{2\pi R}\int_0^{L}\left(\varepsilon^0_y + \frac{w}{R} - \frac{1}{2}w^2_{,y}\right)dxdy = 0 \tag{20}$$

The postbuckling response of stiffened sandwich shells can be effectively analyzed using Eqs. (16), (18), and (20).

4. Solution procedure

This study assesses the effects of stiffeners on the stability of sandwich TSSs under axial loading, assuming simply supported boundary conditions as defined

$$w = 0,\ N_x = 0,\ N_{xy} = 0,\ M_x = 0 \quad x=0,\ x=L \tag{21}$$

To satisfy the given boundary conditions, the shell's deflection, $w(x,y)$, can be approximated by a three-term expression (Huang and Han 2009)

$$w = \xi_0 + \xi_1 \sin\frac{m\pi x}{L}\sin\frac{ny}{R} + \xi_2 \sin^2\frac{m\pi x}{L} \tag{22}$$

Here, m and n represent the buckling modes, while ξ_0, ξ_1, and ξ_2 are the deflection amplitudes. It is evident that the boundary condition (21) is approximately satisfied by the three-term deflection expression (22). By substituting Eq. (22) into Eq. (18), the stress function is defined as

$$\begin{aligned} \phi = \phi_1 \cos\frac{2m\pi x}{L} + \phi_2 \cos\frac{2ny}{R} - \phi_3 \sin\frac{m\pi x}{L}\sin\frac{ny}{R} + \phi_4 \sin\frac{3m\pi x}{L}\sin\frac{ny}{R} \\ -\sigma_{0y}h\frac{x^2}{2} - p_0 h\frac{y^2}{2} \end{aligned} \tag{23}$$

Here, p_0 denotes the compressive axial load, and the ϕ_i expressions (i =1 to 4) are provided by Nam *et al.* (2022). By inserting the stress function (23) and deflection Eq. (22) in Eq. (16), employing the Galerkin method, and taking into consideration Eq. (23), the equilibrium equations, which are expressed algebraically, can be derived as follows

$$v_0 = \frac{S_{32}}{2S_{31}} v_1^2 - \frac{v_2}{2} - \frac{S_{34}}{2S_{31}} p_0 \tag{24}$$

$$S_{11} + S_{12} v_0 + S_{13} v_1^2 + S_{14} v_2 + S_{15} v_2^2 - S_{16} p_0 = 0 \tag{25}$$

$$v_1^2 = \frac{-S_{23} v_2 + S_{24} v_2 p_0}{S_{21} + S_{22} v_2} \tag{26}$$

where S_{11}, S_{12}, S_{14}, S_{15}, S_{16}, S_{22}, S_{23}, S_{24}, and S_{34} are presented by Nam *et al.* (2022). Solving Eqs. (24)-(26) yields the load expression as a function of the nonlinear amplitude, given as follows

$$\begin{aligned} p_0 = &\left[S_{11} + \left(S_{14} - \frac{S_{12}}{2} \right) v_2 + S_{15} v_2^2 - \frac{S_{12} S_{23} S_{32} v_2}{2S_{31}(S_{21} + S_{22} v_2)} - \frac{S_{13} S_{23} v_2}{S_{21} + S_{22} v_2} \right] \\ &\times \left(S_{16} + \frac{S_{12} S_{34}}{2S_{31}} - \frac{S_{13} S_{24} v_2}{S_{21} + S_{22} v_2} - \frac{S_{12} S_{24} S_{32} v_2}{2S_{31}(S_{21} + S_{22} v_2)} \right)^{-1} \end{aligned} \tag{27}$$

By setting $v_2 = 0$, the bifurcation point can be determined as

$$p_0^{upper} = S_{11} / [S_{16} - S_{12} S_{34} / (2S_{31})] \tag{28}$$

The critical buckling load is determined by minimizing the upper buckling load among all modes. From Eqs. (24)-(26), the relationship between maximum deflection and nonlinear amplitude.

$$w_{\max} = \frac{S_{32}(S_{24} v_2 p_0 - S_{23} v_2)}{2S_{31}(S_{21} + S_{22} v_2)} + \frac{v_2}{2} + \left(\frac{S_{24} v_2 p_0 - S_{23} v_2}{S_{21} + S_{22} v_2} \right) - p_0 \frac{S_{34}}{2S_{31}} \tag{29}$$

The postbuckling curves $p_0 - W_{\max}/h$ for stiffened sandwich shells are derived using a combination of Eqs. (27) and (29).

5. Results and discussion

The literature review reveals a lack of research on the buckling and postbuckling characteristics of stiffened sandwich CNT-reinforced TSSs with a GOEAM core under axial compression. Therefore, as part of the validation for the current method, comparative studies are conducted for a specific case of shell geometry and material: a CNTRC cylindrical shell (assuming $a \to \infty$) without stiffeners and an absence of foundation. Compared with Shen and Xiang (2018b), which employs the nonlinear higher-order shear deformation theory, the critical buckling loads of axially compressed CNTRC cylindrical shells in Table 1 are verified. Acceptable agreements are found in this study when the validation cases are examined for various values of $\bar{Z} = L^2/R$. This study presents numerical investigations involving CNTs and the PMMA matrix, as discussed by Shen and Xiang (2018b). Furthermore, the mechanical characteristics of Cu and graphene at 300 *K*, which were used in the buckling analysis of the GOEAM core of sandwich TSSs, are provided by

Table 1 Comparisons of critical buckling load $\bar{p}_{cr} = p_{cr} 2\pi Rh$ (KN) of CNTRC cylindrical shells subjected to axial compression ($h_2 = 0$, h=1 mm, R/h=100, T=300 K)

L^2/Rh	V_{CNT}	Shen and Xiang (2018b)		Present	
		UD	FG-X	UD	FG-X
100	0.12	18.75 (1,7)*	21.81 (1;7)	18.8321 (1,7)	21.638 (1,7)
	0.17	30.43 (1,7)	35.53 (1;7)	30.5419 (1,7)	35.2354 (1,7)
	0.28	37.77 (1,7)	47.18 (1;7)	38.0149 (1,7)	47.2022
300	0.12	19.35 (2,7)	22.06 (1,6)	19.4845 (2,7)	21.9109 (1,6)
	0.17	31.11 (2,7)	37.06 (1,6)	31.2862 (2,7)	36.8317
	0.28	39.60 (2,7)	46.52 (1,6)	39.9881 (2,7)	46.6537

*(*m*,*n*) represent the buckling modes.

Table 2 Comparison of the critical buckling loads (MPa) of stiffened convex sandwich TSSs subjected to axial compression. (H_{Gr}=100%, W_{Gr}=2.5%, L=1.5 R, R/h=80, a=4R, $h_1 = 1$ mm, $h_2 = 2$ mm, $K_1 = 10^7$ N/m^3, $K_2 = 10^5$ N/m, $b_s = b_r = 0.002$ m, $h_s = h_r = 0.003$ m, $n_s = 50, n_r = 12$)

CNT distribution type	V_{CNT}	XD TSS			YD TSS		
		Without stiffener	XD stiffeners	YD stiffeners	Unstiffened	XD stiffeners	YD stiffeners
UD	0.12	459.178 (6,5)	518.582 (5,6)	462.696 (6,6)	258.648 (12,5)	398.601 (8,8)	260.389 (12,6)
	0.17	550.03 (6,5)	612.415 (5,6)	557.163 (6,6)	300.703 (12,6)	472.946 (7,8)	302.09 (12,7)
	0.28	678.622 (5,5)	778.771 (5,5)	688.292 (5,6)	346.978 (12,7)	580.284 (7,8)	347.537 (12,7)
FG-X	0.12	496.441 (6,5)	547.24 (5,6)	500.772 (6,6)	259.712 (12,5)	406.375 (8,8)	261.747 (12,6)
	0.17	593.942 (5,6)	654.755 (5,6)	598.962 (5,6)	303.79 (12,6)	485.355 (7,8)	305.335 (12,6)
	0.28	743.193 (5,5)	832.76 (4,6)	755.068 (5,6)	355.929 (12,7)	602.27 (7,8)	356.608 (12,7)
FG-O	0.12	421.56 (6,6)	479.236 (6,6)	424.791 (6,6)	258.044 (12,5)	391.144 (8,8)	259.503 (12,6)
	0.17	495.669 (6,5)	570.753 (5,6)	501.581 (6,6)	299.136 (12,6)	461.507 (7,8)	299.826 (12,7)
	0.28	616.525 (5,6)	713.154 (5,5)	623.906 (5,6)	343.152 (12,8)	561.669 (6,8)	343.42 (12,8)

Zhao *et al.* (2022a, b, c).

A comprehensive study of the CNT-reinforced shell-stiffener system and its impact on the critical buckling loads of TSSs is presented in Tables 2-3. The results demonstrate that stiffeners significantly enhance the critical buckling loads compared to unstiffened configurations. For instance, a buckling load improvement of 14.76% is observed for convex XD stiffened TSSs relative to unstiffened XD shells, while a 16.83% enhancement is noted for ring-stiffened YD concave TSSs. The numerical findings also reveal that convex FG-CNTRC TSSs exhibit higher critical buckling loads than their concave counterparts. For convex TSSs, longitudinally, CNT-reinforced shells achieve greater critical buckling loads than circumferentially CNT-reinforced

Table 3 Comparison of the critical buckling loads (MPa) of stiffened concave sandwich TSSs subjected to axial compression. (H_{Gr}=100%, W_{Gr}=2.5%, L=1.5R, R/h=80, a=-4R, $h_1 = 1$ mm, $h_2 = 2$ mm, $K_1 = 10^7$ N/m^3, $K_2 = 10^5$ N/m, $b_s = b_r = 0.002$ m, $h_s = h_r = 0.003$ m, $n_s = 50, n_r = 12$)

CNT distribution type		XD TSS			YD TSS		
	V_{CNT}	Unstiffened	XD stiffeners	YD stiffeners	Unstiffened	XD stiffeners	YD stiffeners
UD	0.12	104.815 (1,4)	105.413 (1,4)	116.399 (1,4)	133.6 (1,4)	134.055 (1,4)	146.306 (1,4)
	0.17	107.276 (1,4)	108.201 (1,4)	123.657 (1,4)	149.127 (1,4)	149.787 (1,4)	167.668 (1,4)
	0.28	110.269 (1,4)	111.902 (1,4)	135.339 (1,4)	179.247 (1,4)	180.299 (1,4)	209.422 (1,4)
FG-X	0.12	105.388 (1,4)	106.015 (1,4)	117.36 (1,4)	140.534 (1,4)	141.017 (1,4)	153.626 (1,4)
	0.17	108.186 (1,4)	109.153 (1,4)	125.138 (1,4)	159.328 (1,4)	160.029 (1,4)	178.436 (1,4)
	0.28	111.921 (1,4)	113.623 (1,4)	137.939 (1,4)	195.979 (1,4)	197.099 (1,4)	227.08 (1,4)
FG-O	0.12	104.269 (1,4)	104.838 (1,4)	115.467 (1,4)	126.676 (1,4)	127.102 (1,4)	138.996 (1,4)
	0.17	106.455 (1,4)	107.337 (1,4)	122.271 (1,4)	138.959 (1,4)	139.578 (1,4)	156.934 (1,4)
	0.28	108.941 (1,4)	110.504 (1,4)	133.103 (1,4)	162.637 (1,4)	163.623 (1,4)	191.886 (1,4)

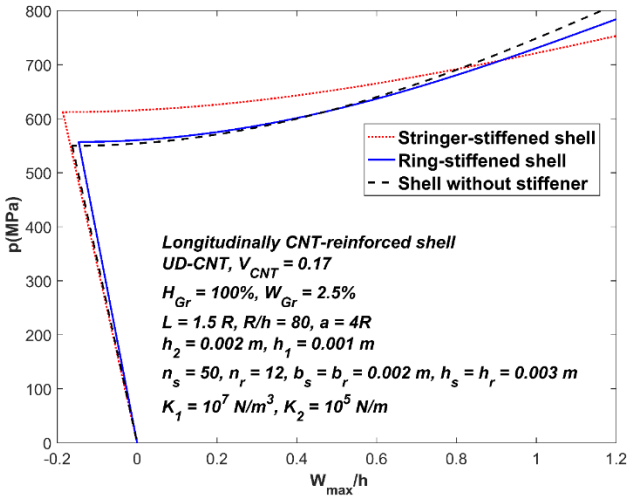

Fig. 4 Impact of stiffeners on the postbuckling paths of convex shells with longitudinal CNT reinforcement

shells. Conversely, concave shells demonstrate higher buckling loads when reinforced circumferentially. Tables 2 and 3 further confirm that, for both shell types, the FG-X CNTRC distribution pattern yields the highest critical buckling loads, while the FG-O pattern results in the lowest. In all cases, increasing CNT content markedly enhances the buckling loads.

Next, stiffeners' effects on the postbuckling curves of GOEAM-core sandwich TSSs are discussed and presented. Figs. 4-7 primarily compare the impact of different types of stiffeners with unstiffened shells for both convex and concave TSSs, considering longitudinally and circumferentially CNT-reinforced shell-stiffener structures, with all cases involving a UD CNT distribution. The significant influence of stiffeners is evident in these investigations. For convex TSSs, as shown in Figs. 4 and 5, the postbuckling curve associated with stringer-type stiffeners occurs at a higher level, while for concave TSSs, the highest postbuckling curve is observed in the ring-stiffened shell (Figs. 6 and 7). Additionally, Figs. 4-5 highlight the complexities of the TSS's

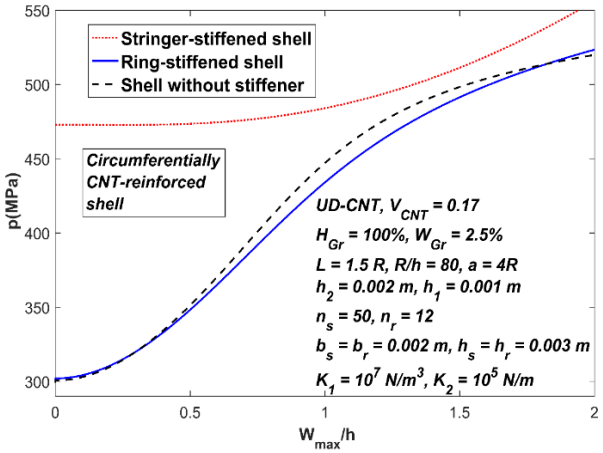

Fig. 5 Impact of stiffeners on the postbuckling paths of convex shells with circumferential CNT reinforcement

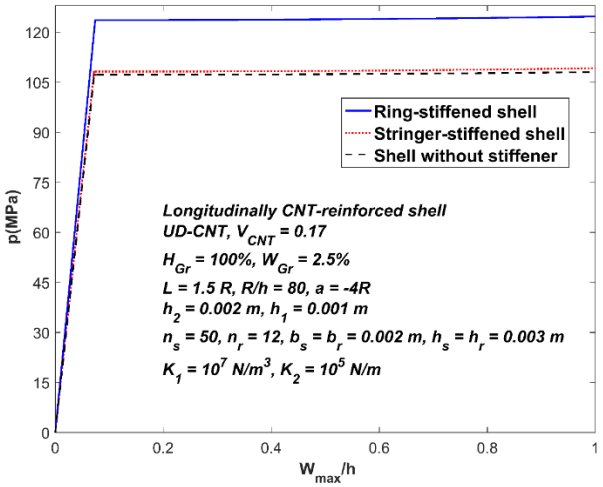

Fig. 6 Impact of stiffeners on the postbuckling response of concave shells with longitudinal CNT reinforcement

nonlinear mechanical characteristics. While the postbuckling trends in concave shells appear regular, the convex shells exhibit significant irregularities. These irregularities may be attributed to material and geometrical complexities, which become more pronounced at higher deflection values.

Figs. 8 and 9 illustrate the impact of CNT distribution types in shell-stiffener structures on the postbuckling characteristics of stiffened TSSs, considering three distinct CNT distribution patterns. The results show a significant enhancement in the postbuckling paths for shells with the FG-X distribution compared to the other patterns. Following FG-X, UD-type shells demonstrate better performance, while FG-O types exhibit the lowest postbuckling strength. Additionally, the snap-through phenomenon is relatively minor in concave TSSs and does not occur in convex shells. Figs. 10 and 11 compare the postbuckling curves of stiffened sandwich TSSs with three

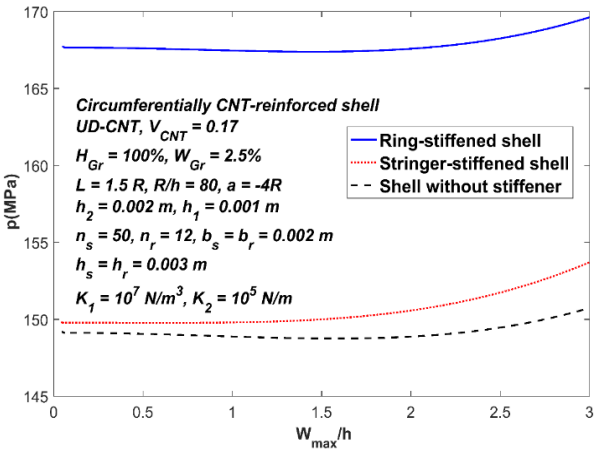

Fig. 7 Impact of stiffeners on the postbuckling response of concave shells with circumferential CNT reinforcement

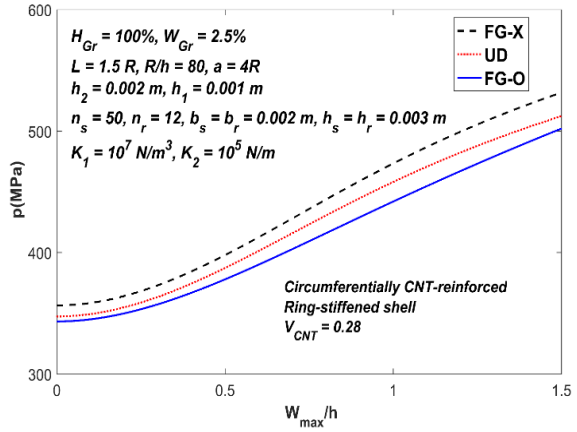

Fig. 8 Impact of CNT distribution models on the postbuckling paths of convex sandwich TSSs

different CNT volume fractions. As shown, the postbuckling strength of the stiffened TSSs increases with higher CNT volume fractions, with these differences becoming more pronounced in the large deflection domain. Typical postbuckling behavior is observed in concave shells. Conversely, the intricate nonlinear mechanical response of convex shells is reflected in their postbuckling paths.

Fig. 12 compares the postbuckling paths of stringer-stiffened shells with varying longitudinal curvatures. The postbuckling paths of TSSs show consistent patterns, while cylindrical shells exhibit a notable snap-through phenomenon. Furthermore, the substantial influence of the geometrical ratio of *R/h* ratio on the buckling and postbuckling characteristics of stiffened GOREAM-core sandwich convex TSSs is demonstrated in Fig. 13. Notably, the critical buckling loads increase significantly as the R/h ratio decreases. Additionally, Fig. 13 reveals distinct patterns in the pre-buckling and postbuckling curves corresponding to different *R/h* ratios.

Figs. 14 and 15 illustrate the influence of elastic foundation stiffness on the stability of stringer-stiffened sandwich GOEAM-core convex and concave TSSs. These figures demonstrate an elastic

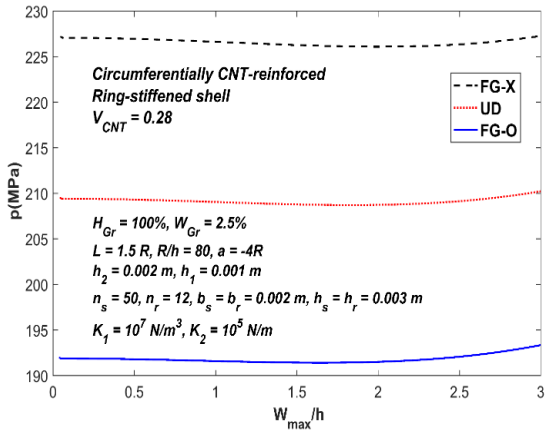

Fig. 9 Impact of CNT distribution models on the postbuckling paths of concave sandwich TSSs

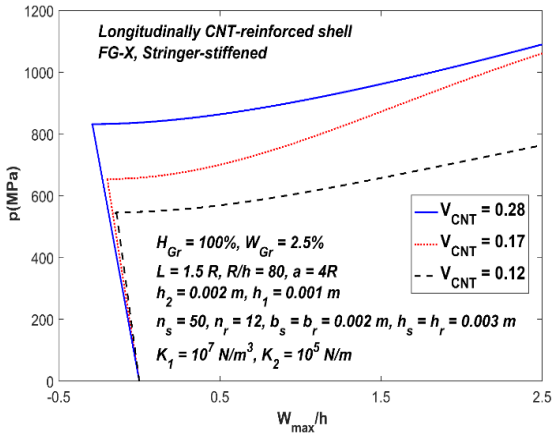

Fig. 10 Impact of CNT content on the postbuckling of convex sandwich TSSs

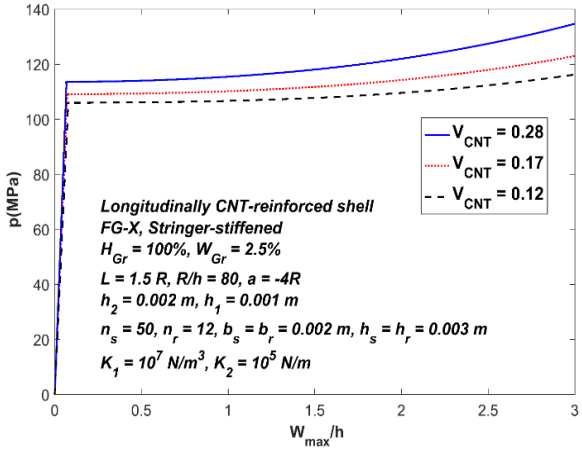

Fig. 11 Impact of CNT content on the postbuckling of concave sandwich TSSs

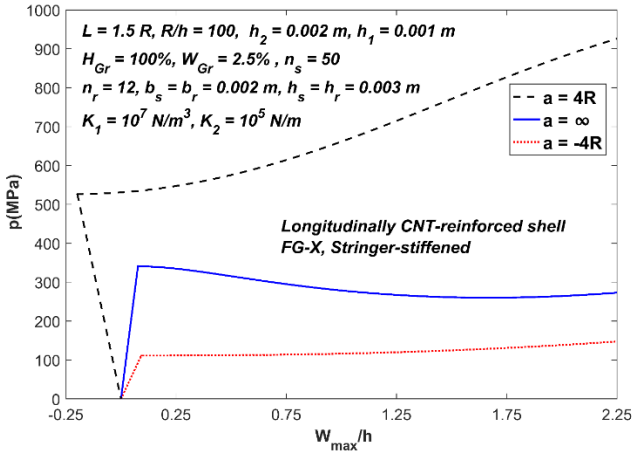

Fig. 12 Impact of longitudinal radius on the postbuckling paths

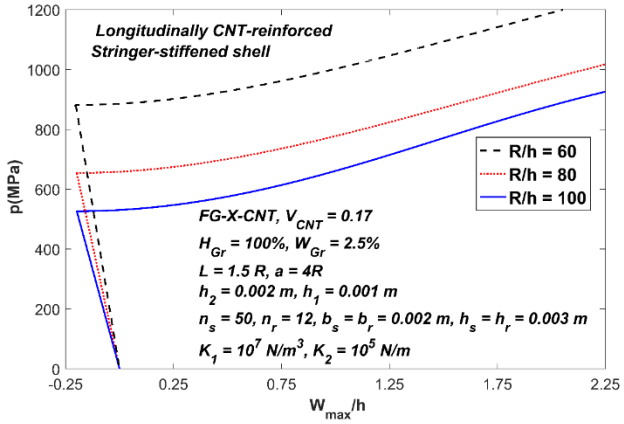

Fig. 13 Impact of R/h ratios on the postbuckling paths of convex sandwich TSSs

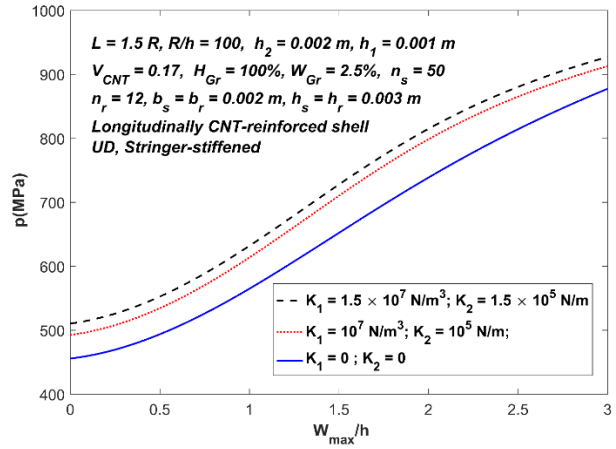

Fig. 14 Impact of elastic foundation on the postbuckling paths of convex sandwich TSSs

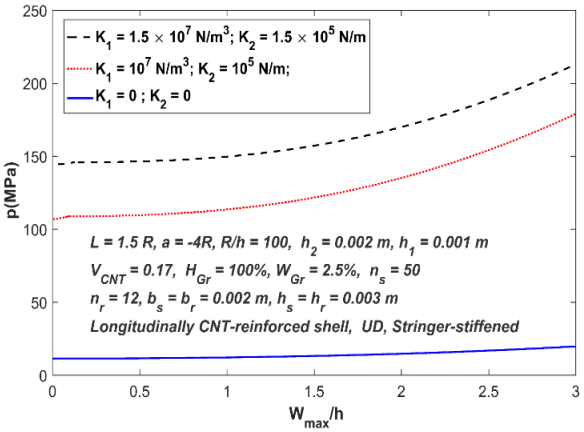

Fig. 15 Impact of elastic foundation on the postbuckling paths of concave sandwich TSSs

foundation's beneficial effect on buckling and postbuckling performance. In particular, elastic foundations enhance load-bearing capacity and reduce the severity of snap-through behavior.

6. Conclusions

This paper investigates the stability of stiffened auxetic-core sandwich TSSs with CNT-reinforced face sheets under axial compression. The study employs Donnell shell theory, von Kármán-type nonlinearity, an innovative smeared stiffener approach for rings and stiffeners, and the Galerkin solution method. The key findings are as follows:

- The critical buckling loads and postbuckling strength of stiffened TSSs are greater than those of unstiffened shells. For instance, a buckling load improvement of 14.76% is observed for convex XD-stiffened TSSs relative to unstiffened XD shells. Similarly, a 16.83% enhancement is noted for ring-stiffened YD concave TSSs.
- The critical buckling loads and postbuckling strength of stiffened convex TSSs are significantly larger than those of stiffened concave TSSs.
- Types of stiffeners, as well as the CNT reinforcement direction of shell-stiffeners structure, strongly influence the critical buckling loads of GOEAM-core sandwich TSSs; for convex TSSs, the critical buckling loads and postbuckling paths are higher when CNT alignment is in the longitudinal direction, and the shells are stiffened longitudinally with stringers stiffeners. Conversely, for concave TSSs, higher buckling loads and elevated postbuckling paths correspond to the circumferentially CNT-reinforced ring-stiffened shells.
- The FG-X CNT distribution model results in the highest buckling load and postbuckling performance among all CNT distribution types.
- As the *R/h* ratio decreases, the critical buckling loads in stiffened convex TSSs increase substantially.
- The presence of an elastic foundation and increased CNT content positively impact the buckling and postbuckling characteristics of TSSs under axial compression load, enhancing load-bearing capacity and reducing the intensity of the snap-through phenomenon.

References

Al-Houri, S., Al-Osta, M.A., Bourada, F., Gawah, Q., Tounsi, A. and Al-Dulaijan, S.U. (2024), "Analysis of porosity-dependent wave propagation in FG-CNTRC beams utilizing an integral higher-order shear deformation theory", *Int. J. Struct. Stab. Dyn.*, 2550233. https://doi.org/10.1142/S0219455425502335.

Cao, V.D., Vu, H.N. and Nguyen, T.P. (2023), "Nonlinear electro-thermo-torsional buckling analysis of stiffened functionally graded graphene-reinforced composite laminated toroidal shell segments", *J. Eng. Mech.*, **149**(2), 04022106. https://doi.org/10.1061/JENMDT.EMENG-6607.

Cho, J.R. (2023), "Investigation of nonlinear free vibration of FG-CNTRC cylindrical panels resting on elastic foundation", *Struct. Eng. Mech.*, **88**(5), 439-449. https://doi.org/10.12989/sem.2023.88.5.439.

Dao, B.H., Dinh, N.G. and Tran, T.I. (2016), "Buckling analysis of eccentrically stiffened functionally graded toroidal shell segments under mechanical load", *J. Eng. Mech.*, **142**(1), 04015054. https://doi.org/10.1061/(ASCE)EM.1943-7889.0000964.

Dong, D.T., Hieu, P.T., Duc, V.M., Phuong, N.T., Tien, N.V. and Nam, V.H. (2023), "Nonlinear buckling analysis of stiffened carbon nanotube-reinforced cylindrical shells subjected to external pressure in thermal environment", *Mech. Compos. Mater.*, **59**(4), 779-794. https://doi.org/10.1007/s11029-023-10131-9.

Dong, D.T., Nam, V.H., Phuong, N.T., Ly, L.N., Duc, V.M., Van Tien, N., ... & Quan, P.H. (2022), "An analytical approach of nonlinear buckling behavior of longitudinally compressed carbon nanotube-reinforced (CNTR) cylindrical shells with CNTR stiffeners in thermal environment", *ZAMM-J. Appl Math. Mech./Zeitschrift für Angewandte Mathematik und Mechanik*, **102**(4), e202100228. https://doi.org/10.1002/zamm.202100228.

Dong, Y.H., He, L.W., Wang, L., Li, Y.H. and Yang, J. (2018), "Buckling of spinning functionally graded graphene reinforced porous nanocomposite cylindrical shells: an analytical study", *Aerosp. Sci. Technol.*, **82**, 466-478. https://doi.org/10.1016/j.ast.2018.09.037.

Ebrahimi, F. (2015). *Graphene: New Trends and Developments*, BoD-Books on Demand.

Ebrahimi, F. (2024), *Mechanics of Auxetic Materials and Structures*, CRC Press.

Ebrahimi, F. and Ahari, M.F. (2024), "On the buckling of meta-graphene-origami-enabled magnetostrictive nanoplates under temperature gradient", *Acta Mechanica*, **235**, 2611-2628. http://dx.doi.org/10.1007/s00707-024-03861-x.

Ebrahimi, F. and Dabbagh, A. (2020), *Mechanics of Nanocomposites: Homogenization and Analysis*, CRC Press.

Ebrahimi, F. and Dadashi, M. (2023), "Composite cylindrical shells with auxetic core on elastic foundation: A nonlinear dynamic analysis", *Struct.*, **57**, 105170. http://dx.doi.org/10.1016/j.istruc.2023.105170.

Ebrahimi, F. and Ezzati, H. (2024), "Dynamic analysis of thermally affected nanocomposite plates reinforced with functionalized graphene oxide nanoparticles", *Acta Mechanica*, **235**(1), 337-354. https://doi.org/10.1007/s00707-023-03754-5.

Ebrahimi, F. and Parsi, M. (2023), "Wave propagation analysis of functionally graded graphene origami-enabled auxetic metamaterial beams resting on an elastic foundation", *Acta Mechanica*, **234**(12), 6169-6190. http://doi.org/10.1007/s00707-023-03705-0.

Ebrahimi, F., Effatmaneshfard, A., Ezzati, H. and Pashalou, S. (2024a), "Stability analysis of functionally graded graphene platelets-reinforced nanocomposite shells", *J. Comput. Appl. Mech.*, **55**(3), 355-368. https://doi.org/10.22059/jcamech.2024.373854.999.

Ebrahimi, F., Goudarzfallahi, M. and Ziazi, A.A. (2024b), "Static stability analysis of graphene origami-reinforced nanocomposite toroidal shells with various auxetic cores", *Adv. Nano Res.*, **17**(1), 1. https://doi.org/10.12989/anr.2024.17.1.001.

Ebrahimi, F., Goudarzfallahi, M. and Ziazi, A.A. (2024c), "Porosity effects on the buckling and post buckling of metamaterial sandwich toroidal shell segments", *Steel Compos. Struct.*, **53**(3), 313-326. https://doi.org/10.12989/scs.2024.53.3.313.

Fu, T., Hu, X. and Yang, C. (2023), "Impact response analysis of stiffened sandwich functionally graded

porous materials doubly-curved shell with re-entrant honeycomb auxetic core", *Appl. Math. Model.*, **124**, 553-575. https://doi.org/10.1016/j.apm.2023.08.024.

Hieu, P.T. and Tung, H.V. (2020), "Postbuckling behavior of carbon-nanotube-reinforced composite toroidal shell segments subjected to thermomechanical loadings", *AIAA J.*, **58**(7), 3187-3198. https://doi.org/10.2514/1.j059055.

Huang, H. and Han, Q. (2009), "Nonlinear elastic buckling and postbuckling of axially compressed functionally graded cylindrical shells", *Int. J. Mech. Sci.*, **51**(7), 500-507. https://doi.org/10.1016/j.ijmecsci.2009.05.002.

Jin, X., Huang, X., Chen, Y. and Wang, H. (2024), "Thickness-stretched model for thermal vibrational behaviors of graphene origami reinforced doubly curved", *J. Therm. Stress.*, **47**(4), 502-520. http://dx.doi.org/10.1080/01495739.2024.2325980.

Kamrava, S., Mousanezhad, D., Ebrahimi, H., Ghosh, R. and Vaziri, A. (2017), "Origami-based cellular metamaterial with auxetic, bistable, and self-locking properties", *Scientif. Report.*, **7**(1), 46046. https://doi.org/10.1038/srep46046.

Kolken, H.M. and Zadpoor, A.A. (2017), "Auxetic mechanical metamaterials", *RSC Adv.*, **7**(9), 5111-5129. https://doi.org/10.1039/C6RA27333E.

Minh, T.Q., Duc, V.M. and Phuong, N.T. (2022), "Nonlinear buckling behavior of FG-CNTRC toroidal shell segments stiffened by FG-CNTRC stiffeners under external pressure", *Modern Mech. Appl.: Select Proceedings of ICOMMA*, **2020**, 240-255. http://doi.org/10.1007/978-981-16-3239-6_19.

Murari, B., Zhao, S., Zhang, Y. and Yang, J. (2024), "Machine learning-assisted vibration analysis of graphene-origami metamaterial beams immersed in viscous fluids", *Thin Wall. Struct.*, **197**, 111663. https://doi.org/10.1016/j.tws.2024.111663.

Nam, V.H., Duc, V.M., Doan, C.V., Xuan, N.T. and Phuong, N.T. (2022), "Nonlinear postbuckling behavior of auxetic-core toroidal shell segments with Graphene reinforced face sheets under axial loads", *Arch. Mech.*, **74**(2-3), 89-108. http://doi.org/10.24423/aom.3957.

Nguyen, T.P., Vu, M.D., Dang, T.D., Cao, V.D., Pham, T.H. and Vu, H.N. (2023), "An analytical approach of nonlinear buckling behavior of torsionally loaded auxetic core toroidal shell segments with graphene reinforced polymer coatings", *Adv. Compos. Mater.*, **32**(3), 400-418. http://doi.org/10.1080/09243046.2022.2110661.

Phuong, N.T., Trung, N.T., Van Doan, C., Thang, N.D., Duc, V.M. and Nam, V.H. (2020), "Nonlinear thermomechanical buckling of FG-GRC laminated cylindrical shells stiffened by FG-GRC stiffeners subjected to external pressure", *Acta Mechanica*, **231**(12), 5125-5144. https://doi.org/10.1007/s00707-020-02813-5.

Phuong, N.T., Van Doan, C., Duc, V.M., Giang, N.T. and Nam, V.H. (2023), "Analytical solution for nonlinear buckling of convex and concave auxetic-core toroidal shell segments with graphene-reinforced face sheets subjected to radial loads", *Arch. Appl. Mech.*, **93**(2), 621-634. http://doi.org/10.1007/s00419-022-02288-x.

Reddy, J.N. (2003), *Mechanics of Laminated Composite Plates and Shells: Theory and Analysis*, CRC Press.

Reddy, J.N. and Starnes Jr, J.H. (1993), "General buckling of stiffened circular cylindrical shells according to a layerwise theory", *Comput. Struct.*, **49**(4), 605-616. https://doi.org/10.1016/0045-7949(93)90065-L.

Sahmani, S. and Aghdam, M.M. (2017), "Nonlinear instability of axially loaded functionally graded multilayer graphene platelet-reinforced nanoshells based on nonlocal strain gradient elasticity theory", *Int. J. Mech. Sci.*, **131**, 95-106. https://doi.org/10.1016/j.ijmecsci.2017.06.052.

Shen, H.S. (2011), "Postbuckling of nanotube-reinforced composite cylindrical shells in thermal environments, Part I: Axially-loaded shells", *Compos. Struct.*, **93**(8), 2096-2108. https://doi.org/10.1016/j.compstruct.2011.02.011.

Shen, H.S. and Xiang, Y. (2018a), "Postbuckling behavior of functionally graded graphene-reinforced composite laminated cylindrical shells under axial compression in thermal environments", *Comput. Meth. Appl. Mech. Eng.*, **330**, 64-82. http://doi.org/10.1016/j.cma.2017.10.022.

Shen, H.S. and Xiang, Y. (2018b), "Postbuckling of functionally graded graphene-reinforced composite laminated cylindrical shells subjected to external pressure in thermal environments", *Thin Wall. Struct.*,

124, 151-160. https://doi.org/10.1016/j.tws.2017.12.005.
Shen, H.S., Xiang, Y. and Lin, F. (2017), "Nonlinear bending of functionally graded graphene-reinforced composite laminated plates resting on elastic foundations in thermal environments", *Compos. Struct.*, **170**, 80-90. https://doi.org/10.1016/j.compositesb.2017.10.032.
Sofiyev, A.H. and Kuruoglu, N.U.R.İ. (2022), "Buckling analysis of shear deformable composite conical shells reinforced by CNTs subjected to combined loading on the two-parameter elastic foundation", *Def. Technol.*, **18**(2), 205-218. https://doi.org/10.1016/j.dt.2020.12.007.
Stein, M. and McElman, J.A. (1965), "Buckling of segments of toroidal shells", *AIAA J.*, **3**(9), 1704-1709. https://doi.org/10.2514/3.55185.
Thang, P.T., Kim, H., Kim, C., Jang, H., Kim, T. and Kim, J. (2024), "Free vibration analysis of barrel-shaped sandwich shells with auxetic honeycomb core using modified thick shell theory", *Aerosp. Sci. Technol.*, **145**, 108861. http://dx.doi.org/10.1016/j.ast.2023.108861.
Torabi, J. and Ansari, R. (2018), "Thermally induced mechanical analysis of temperature-dependent FG-CNTRC conical shells", *Struct. Eng. Mech.*, **68**(3), 313-323. https://doi.org/10.12989/sem.2018.68.3.313.
Van Tien, N., Duc, V.M., Nam, V.H., Phuong, N.T., Ho, L.S., Dong, D.T., ... & Minh, T.Q. (2022), "Nonlinear postbuckling of auxetic-core sandwich toroidal shell segments with CNT-reinforced face sheets under external pressure", *Int. J. Struct. Stab. Dyn.*, **22**(01), 2250006. http://doi.org/10.1142/S0219455422500067.
Vuong, P.M. and Duc, N.D. (2018), "Nonlinear response and buckling analysis of eccentrically stiffened FGM toroidal shell segments in thermal environment", *Aerosp. Sci. Technol.*, **79**, 383-398. http://doi.org/10.1016/j.ast.2018.05.058.
Wang, B., Tian, K., Hao, P., Zheng, Y., Ma, Y. and Wang, J. (2016), "Numerical-based smeared stiffener method for global buckling analysis of grid-stiffened composite cylindrical shells", *Compos. Struct.*, **152**, 807-815. https://doi.org/10.1016/j.compstruct.2016.05.096.
Wang, Y., Xie, K. and Fu, T. (2020), "Size-dependent dynamic stability of a FG polymer microbeam reinforced by graphene oxides", *Struct. Eng. Mech.*, **73**(6), 685-698. https://doi.org/10.12989/sem.2020.73.6.685.
Xu, J.Q. and She, G.L. (2023), "Thermal post-buckling of graphene platelet reinforced metal foams doubly curved shells with geometric imperfection", *Struct. Eng. Mech.*, **87**(1), 85-94. https://doi.org/10.12989/sem.2023.87.1.085.
Zhai, Z., Wu, L. and Jiang, H. (2021), "Mechanical metamaterials based on origami and kirigami", *Appl. Phys. Rev.*, **8(**4), 41319 http://doi.org/10.1063/5.0051088.
Zhao, S., Zhang, Y., Wu, H., Zhang, Y. and Yang, J. (2022c), "Functionally graded graphene origami-enabled auxetic metamaterial beams with tunable buckling and postbuckling resistance", *Eng. Struct.*, **268**, 114763. https://doi.org/10.1016/j.engstruct.2022.114763.
Zhao, S., Zhang, Y., Zhang, Y., Yang, J. and Kitipornchai, S. (2022b), "Vibrational characteristics of functionally graded graphene origami-enabled auxetic metamaterial beams based on machine learning assisted models", *Aerosp. Sci. Technol.*, **130**, 107906. https://doi.org/10.1016/j.ast.2022.107906.
Zhao, S., Zhang, Y., Zhang, Y., Zhang, W., Yang, J. and Kitipornchai, S. (2022a), "Genetic programming-assisted micromechanical models of graphene origami-enabled metal metamaterials", *Acta Materialia*, **228**, 117791. https://doi.org/10.1016/j.actamat.2022.117791.
Zhou, Z., Ni, Y., Tong, Z., Zhu, S., Sun, J. and Xu, X. (2019), "Accurate nonlinear buckling analysis of functionally graded porous graphene platelet reinforced composite cylindrical shells", *Int. J. Mech. Sci.*, **151**, 537-550. https://doi.org/10.1016/j.ijmecsci.2018.12.012.